Definition of a Non-contact Induction Heating of a Cutting Tool as a Substitute for the Process Heat for the Verification of a Thermal Simulation Model

Lukáš Topinka[1(✉)], Radomír Pruša[2], Rostislav Huzlík[2], and Joachim Regel[1]

[1] Institute for Machine Tools and Production Processes (IWP), Chemnitz University of Technology, Chemnitz, Germany
`lukas.topinka@mb.tu-chemnitz.de`
[2] Institute of Production Machines, Systems and Robotics, Brno University of Technology, Brno, Czech Republic

Abstract. During metal machining, a large amount of heat is generated in the cutting zone, which has a negative impact on machining accuracy due to the thermal expansion of the materials. To reduce the temperature in the cutting zone, liquid coolants are used which increase the costs and can have a negative impact on the environment. This problem is being studied using Computational Fluid Dynamics (CFD) to better understand the behavior of the coolant flow in the cutting zone, which will allow optimization of the use of liquid coolants and the development of a correction method for thermal errors, resulting in more accurate machining with reduced resource and environmental footprints. However, due to the complexity of multiphase CFD simulations, the simulation model must be simplified as much as possible. This is particularly important for the process heat generation, as combining flow simulation of coolant flow around the rotating cutting tool with structural simulation of the milling process, including chip formation, would require excessive computational power. In following paper an alternative method of tool heating by electromagnetic induction is presented and the measurement dependencies required to determine the heat flux induced into the cutting tool are described. This can be further applied as a boundary condition for the numerical simulation as a verification method for the coupled Fluid-Structure Interaction FSI simulation model of the thermally induced deformations of the cutting tool and its holder.

Keywords: Thermal error · Cutting tool · Induction heating

1 Introduction

During a milling process, the tool engages the workpiece and removes material in the form of chips to achieve the final shape of the workpiece. This chip removal is caused by plastic deformation of the workpiece material due to high machining forces, which results in high frictional forces between the tool and the workpiece. This causes a large

amount of heat generated in the cutting zone. The generated heat is largely removed through the chips, but some of the heat is accumulated in the tool, causing its thermal deformation. This has a negative effect on the dimensional accuracy of the machined workpiece, and thereby reduces the efficiency of the machining itself.

Today, liquid cooling is a standard for a wide range of cutting processes. In addition to cooling the cutting zone itself, the use of a liquid coolant affects chip formation and friction between the cutting tool and the workpiece, thus changing heat transfer and reducing heat generation in the cutting zone [1, 2]. The use of cutting fluids not only increases the cost of a given machining process, but also reduces its environmental friendliness. However, simply reducing the amount of cutting fluid in the cutting zone can negatively affect the entire process and increase the dimensional variation of the workpiece due to thermal deformations.

In order to improve the efficiency of machining processes, the SFB/Transregio96 cooperative project has been set up, where the influence of different cooling strategies on the thermal behaviour of the cutting tool and thus its dimensional deviation is being investigated in subproject A01, mainly by means of numerical simulations. The aim of this subproject is not only to increase the efficiency of the use of cutting fluids and thus reducing both machining costs and environmental burden, but also to develop a correction method for thermal errors during the machining process itself and thus enable more accurate machining.

The simulation model is being developed within the framework of subproject A01 to simulate different cooling methods of cutting tools combines fluid (CFD), thermal and structural simulations within a Fluid Structure Interaction (FSI) coupling, as introduced in [3]. This simulation model has to be experimentally verified using real measured data to verify the accuracy of the simulated results.

The first stage is a fluid simulation of the coolant flow. Due to the complexity of fluid simulations in combination with vortex and turbulent flows around a rotating tool, the simulation model needs to be simplified as much as possible, i.e. only the components necessary to simulate the problem should be included, as described in [4]. After the functional fluid simulation, the thermal conditions need to be set to simulate the effectiveness of the different cooling strategies.

To verify thermal simulations, suitable boundary conditions must be defined that can be compared with the experimental measurements. These include stable and defined ambient conditions, which is why such investigations are often carried out in an isolated climate cell [5], as well as the accurate definition of the heat input in the machine structure like heating mats as a substitute for planar or punctual heat sources [6]. Since simulating the real cutting process including chip removal would be too time consuming and therefore inefficient, an alternative heating method must be developed that will supply a defined amount of heat to the tool while allowing the tool to rotate and not affecting other factors such as coolant flow. There are various ways of heating the cutting tool as a substitute for the heat from the cutting zone with the possibility of defining the heat flux into the cutting tool, e.g. heating rod, laser or induction heating. This article describes a method for heating the cutting tool by an electromagnetic induction and determining the heat input based on current and power measurements on the inductor and supported by an electromagnetic simulation.

2 Induction Heating and Design Boundary Conditions

Induction heating is described by Faraday's law of induction, which function is similar to that of a transformer. The primary winding is supplied with alternating current and emits an electromagnetic field. The heated object represents the secondary winding and receives the radiated magnetic field. According to the previously mentioned Faraday's law, a voltage is induced in the object and eddy currents are generated. Due to the eddy currents, Joule heat is released, i.e. the energy of electromagnetic radiation is converted into thermal energy. Heating by induction does not occur uniformly throughout the volume, but depends on the so-called penetration depth δ. The penetration depth is calculated according to the equation:

$$\delta = \sqrt{\frac{2}{\omega \cdot \mu \cdot \sigma}} \tag{1}$$

where ω is the angular velocity, μ is the magnetic permeability and σ is the specific electrical conductivity [7]. From the point of view of efficiency, the penetration depth is also important, since 99.6% of the total energy in the material is dissipated in three times the penetration depth [8]. For penetration depth, it is 86.5% of the energy [8]. In the case of magnetic simulations, it is necessary to keep this fact in mind and focus on that area.

Induction heating was found to be suitable for simulated heating of the cutting tool as it allows non-contact heating. This allows the cutting tool to rotate and be cooled by the liquid, so simplified boundary conditions can be used for the CFD simulation model. However, it is necessary to establish the basic criteria that the primary inductor coil should meet. The coil should have a sufficient inner diameter to ensure there is enough space between the coil and the tool so that the fluid flow around the tool is not affected by the position of the coil. On the other hand, a smaller coil diameter results in a better energy transfer to the tool and therefore a more effective tool heating. For this purpose, an inductor coil with an inner diameter of 56 mm was wound from a copper wire with a circular cross-section and a diameter of 1.8 mm. From the point of view of tool heating in machining, it is desirable that only a certain area is heated. The length of the primary coil must be as short as possible so that most of the heating power can be applied near the tip of the tool. Therefore, a coil with three wiring in two layers was designed, which enables the length of the coil to be reduced to only 8 mm, but also provides a small distance between the wires and thus a better flow of ambient air, helping in cooling the coil, as the coil was not internally cooled.

3 Determination of Heating Power

In the first step, a substitute tool model with a simplified shape was chosen instead of a further used end mill tool. The substitute was a cylinder with an outer diameter of 20 mm and a length of 105 mm, corresponding with the dimensions of the end mill tool. That simplifies the boundary conditions for the first version of an electromagnetic simulation model and avoids systematic errors in measurements and simulations due to the rotationally symmetrical shape of the test cylinder. The material of this test cylinder as well as of the further used end mill was HSS-E.

To provide the necessary conditions for the implementation and verification of the heating functionality, an experimental test stand was created, which is schematically shown in Fig. 1. The test stand can be divided into two sides - the power supply and the measurement section. The power supply section consists of a DC power supply for the frequency converter. At the end of the circuit the primary coil was constructed as described in the previous section. The frequency converter is based on a bistable oscillating circuit. The output sinusoidal signal is achieved by resonance between the capacitors and the primary inductor coil.
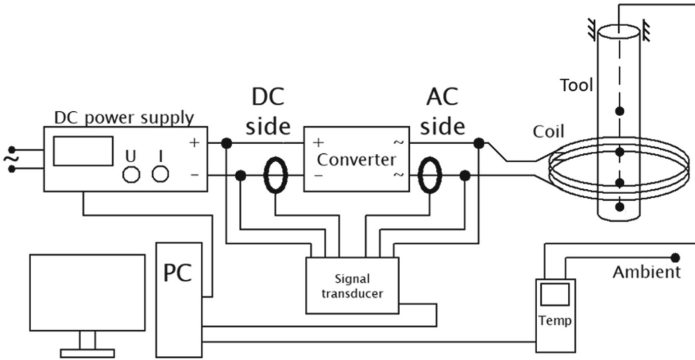
Fig. 1. Schematic arrangement of the measuring test stand

The measured electrical parameters were voltages and currents on DC and AC side. The determination of the electrical power on the DC side was easy and accurate. On the other hand, the determination of the power on the AC side was complicated. This was due to the limited accuracy of the high frequency current measurement. The converter was set to output at 40 kHz. Most current transducers have a given bandwidth, i.e. the waveform and magnitude are not problematic to determine. The calculation of electrical power results from the instantaneous voltage and current. For a valid power quantity, not only an exact amplitude value but also time accuracy, i.e. the phase shift between voltage and current, is required, as described in [9]. The selected power configurations on the DC side and the measured values on the AC side for this validation approach are given in Table 1. These power values were selected after a few probe measurements with the aim of not exceeding 100 °C, which was sufficient for the verification of the described methodology. For verification, it was not necessary to reach higher hundreds of degrees Celsius, as this could damage the plastic fixture used and thus reduce the reliability of the verification.

Table 1. Selection of power configuration and measured values test cylinder

$P_{DC}[W]$	$U_{DC}[V]$	$I_{DC}[A]$	$I_{pk-pk}[A]$	$f[kHz]$
6.5	3.91	1.67	22.4	39.47
8.2	4.26	1.93	25.5	39.39
10.1	4.59	2.21	28.6	39.34
12.2	4.94	2.47	31.4	39.29

3.1   Electromagnetic Simulation and Verification of Heating Power

In the second step, a 3D model of the induction coil and the heated object was created in the environment of ANSYS Maxwell® with the configuration based on the experimental test stand. This model simulates the electromagnetic field and resulting ohmic losses causing the heating of the object. The coil model has been simplified as the supply wires have not been considered. From a simulation point of view, this simplifies the creation of the mesh, since the possible error due to field asymmetry is negligible.

To be able to prove the correctness of the simulation model, the heated object in the first series of the simulations was a test cylinder. The basic shape of the cylinder enabled to verify the precision of the simulated results analytically. The dimensions and material of the test cylinder were chosen to correspond with further used end mill tool. The unknown electromagnetic properties, such as permeability, were defined based on the material steel_1010 from the ANSYS Maxwell® material library, which was the nearest to HSS-E from the available material data. This enabled to compare the transmitted energy for both test objects. The input boundary parameters were the amplitude of the measured current on the AC side and the measured frequency obtained on the previously described test stand (see Fig. 1).

Initial verification of the electromagnetic simulation was based on two main parameters – penetration depth δ, described in Sect. 2, and the calculated ohmic losses in the test object caused by eddy currents. For the basic test cylinder, these parameters could be analytically determined and thus compared with simulated results. For this verification, it was necessary to measure the total power delivered to the circuit and determine the heating power transmitted to the test object among other loss components. The total power measured on the DC side consists of following components:

- power dissipated by the frequency converter ΔP_C
- power dissipated by the supply cables ΔP_w
- ohmic losses of the main induction coil ΔP_J
- power transmitted by leakage magnetic fluxes to the surrounding environment and objects ΔP_o
- power transmitted to the body under test P.

All the listed power components could not be exactly identified or calculated. However, some of them could be neglected, as their percentage share is negligible compared to the other components. Since the efficiency of inverters is generally around 95% [10], the loss ΔP_C could be neglected. The DC supply cable was short with conductors of

sufficient cross section, therefore the losses ΔP_w could also be neglected. Due to the sufficient distance from all metallic objects and the large magnetic conductivity of the test object, the loss due to leakage magnetic fluxes ΔP_o was also negligible. On the other hand, the loss on the main induction coil ΔP_J cannot be neglected, because the coil also heats up during the measurements, which means a significant part of a total energy is transmitted into the heating energy of the coil. Based on the previous assumptions, the total power delivered to the test object P can be calculated according to the following equation:

$$P = U_{DC} \cdot I_{DC} - R \cdot I_{RMS}^2 \tag{2}$$

where R is the resistance value of the main induction coil, I_{RMS} is the effective current value on the AC side. When measuring the resistance of the induction coil, it was necessary to consider the increase in resistance due to the skin effect. For this reason, it was necessary to measure the magnitude using e.g. a milliohmmeter to adjust the measuring magnitude of the frequency at which the measurement will take place. According to Table 1, the supply frequency on the AC side was around 40 kHz. The resulting measured value was 20 mOhm. Furthermore, it was important to measure the resistance without the presence of the test object, otherwise the measured resistance would be increased by the iron losses occurring in this object. Table 2 shows the values obtained from the simulation of the electromagnetic field and the measurement and subsequent calculation for the test cylinder.

Table 2. Comparison of simulated and calculated ohmic losses for the test cylinder

Measurement			Simulation		Difference
$P_{DC}[W]$	$P_J[W]$	$P_M[W]$	$P_J[W]$	$P_S[W]$	$P_{M-S}[W]$
6.5	1.2	5.3	1.4	4.9	0.4
8.2	1.6	6.6	1.9	6.3	0.3
10.1	2.0	8.1	2.3	7.9	0.2
12.2	2.5	9.7	2.8	9.5	0.2

The result in Table 2 present that the power obtained from the measurement was higher than the simulated power. This confirms the fact, that the measured power included the neglected losses (ΔP_C, ΔP_w, ΔP_o) and thus resulted to slightly higher values of power dissipated into the test object. Furthermore, it can also be noticed that about 20% of the total power was dissipated in the main induction coil, causing its heating. Figure 2 shows an example of the solution for the power of 10,1 W on the DC side, specifically the representation of the ohmic losses in the test object. It is apparent that most power is transferred near to the coil position, where the electromagnetic field is strongest. Moreover, in the frontal cross-section it can be seen that the energy is mainly transferred only in the thin layer (penetration depth δ), which is confirming the information given before.
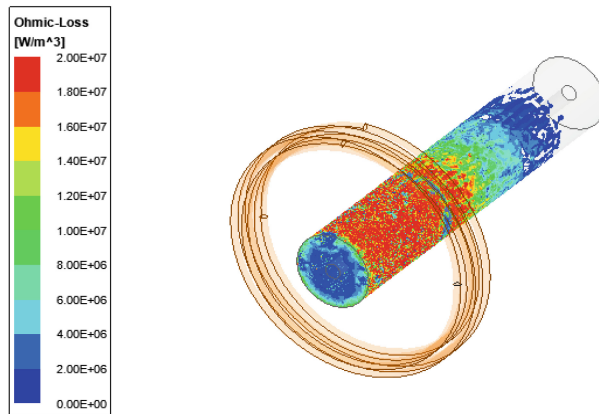
Fig. 2. Simulation results of ohmic loss in the test cylinder for DC power 10.1 W in ANSYS Maxwell®

## 3.2 Simulation of the Heating Power of an End Mill Tool

After the electromagnetic simulation of the basic test cylinder had been verified and its results were reliable, the model of the heated test cylinder could be replaced. The new heated object was a four-edged end mill, which was used for the investigations described in Sect. 1. The dimensions of the previously used test cylinder, corresponding to those of the end mill, allowed easy replacement, while keeping the coil position and the experimental setup the same, so that a comparison between both heated objects was possible. The experimental test stand with the end mill is shown in Fig. 3.

Fig. 3. Experimental setup on test stand with end mill tool

The same series of the previously described measurements was carried out on the test stand with the real end mill tool, made from the same material as the previous test cylinder, in order to obtain initial boundary conditions for the simulation. An example of simulated results in Fig. 4 shows similar distribution of the acting field, respectively

ohmic losses as in the previous simulation with the basic cylinder. This is caused by the electromagnetic field created around the main induction coil, which behaved similarly in both cases.
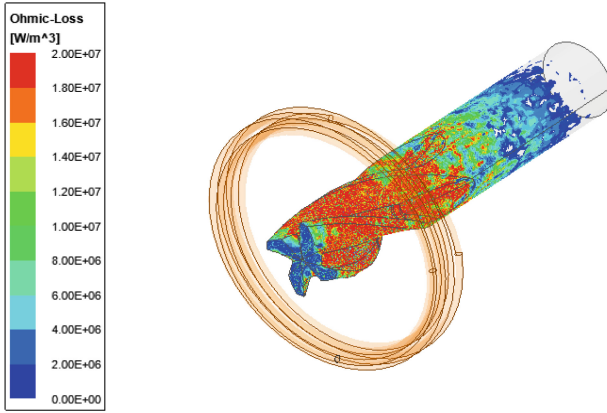
Fig. 4. Simulation results of ohmic loss in the end mill for DC power 10.1 W in ANSYS Maxwell®

The power dissipation into the end mill was also calculated based on the measured data and the Eq. (2). However, in comparison to the values obtained for the test cylinder, a slightly lower efficiency of heating purpose can be seen, as the power dissipated into the end mill tool was around 75–78% of the total power on the DC side, as shown in Table 3.

Table 3. Comparison of simulated and calculated ohmic losses for the end mill

Measurement			Simulation		Difference
$P_{DC}[W]$	$P_J[W]$	$P_M[W]$	$P_J[W]$	$P_S[W]$	$P_{M-S}[W]$
6.5	1.4	5.1	1.6	4.5	0.6
8.2	1.9	6.3	2.2	5.8	0.5
10.1	2.3	7.8	2.7	7.3	0.5
12.2	2.9	9.3	3.4	8.9	0.4

It should be noted that the resulting deviation of the results for both the test cylinder and the end mill tool may be caused not only by the simplified and thus slightly different shape and volume of the heated objects, but also by inaccuracies in the measurement process and due to the slightly simplified simulation models and boundary conditions. In the calculated differences P_{M-S}, the tendency can be seen that the difference decreases with increasing power configuration. However, the aim of this study was to find out whether it is possible to define the heating power as heat input into the simulation model

when using induction heating, and thus to use and further develop this methodology. The further goal is to tend rather to higher reached temperatures, and thus to use higher heating powers. There, the difference between experimental measurements and simulations is smaller and therefore the further investigation on finding the most influencing factor for these deviations was not carried out.

4   Thermal Simulation

The simulated ohmic losses from the previous electromagnetic simulation were exported as a 3D field based on Cartesian coordinates. This data file was further imported into a thermal simulation model as an input boundary condition for the simulated heating of the tested end mill. The comparison of these simulated thermal results and measured temperatures on the test stand (as described in Sect. 1) was the last step to prove the functionality of this methodology.

The thermal simulation model was created in the ANSYS CFX in a similar way as the FSI simulation model mentioned earlier in this article. Since the plastic fixture has only a few contact surfaces with the heated end mill, its presence in the simulation model would have minimal effect on the simulated temperatures but would increase the meshing requirements of the model and thus increase the calculation time. The same applies to the coil near the end mill tip, as it can slightly affect the flowing air, but not in such a way that it would influence the simulated temperatures. For this reason, both parts were neglected in the simulation model, which simplifies the conditions for meshing and allows faster and smoother convergence of the simulation model without significantly affecting the simulated results. Therefore, the thermal simulation model contained only a 3D model of tested end mill tool and a small ambient air area. The material parameters were defined according to the material properties of the HSS-E end mill on the test stand with a thermal conductivity of 27,4 W/mK and a specific heat capacity of 420 J/kgK.
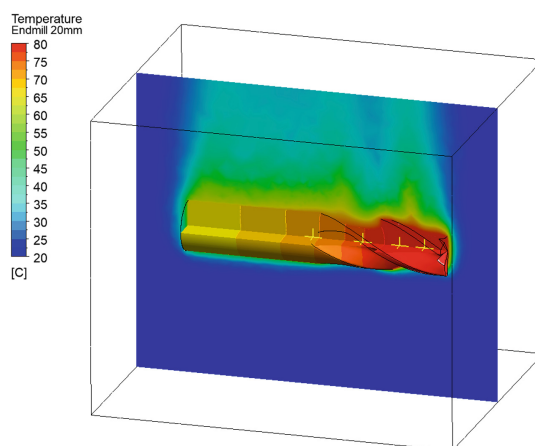
Fig. 5. Simulated temperature field of the end mill for set power of 10.1 W on the DC side in ANSYS CFX

Figure 5 shows an example of a resulting color map of the simulated temperature field of the end mill and ambient air from the steady-state simulation with marked positions of the read temperatures for power of 10,1 W on DC side.

The steady-state thermal simulations were carried out for the same series of power values as the electromagnetic simulations. In order to verify the results, the temperature profile on the tested end mill was measured during induction heating with four PT 100 sensors implemented into the tested tool. These sensors were placed into a small hole drilled along the rotational axis in the distances of 10, 20, 35 and 55 mm from the top face on the coil side. The position of the sensors along the axis of the tested object minimizes the possible influence of electromagnetic field as it acts just under the surface of the tool. The entire test setup was placed in a closed test stand, where the ambient temperature was measured so that the boundary conditions were stable and defined. The measurement time interval was 120 min. Although the measured time interval exceeds most milling operations, it was necessary to heat the tested tool fully to achieve a steady-state thermal condition for proper verification of the simulation model, since comparing only a few seconds of measured heating curve would not be sufficient for proper verification and would require transient simulation. The resulting steady-state temperatures could be compared with the simulated temperature values at positions corresponding to the position of the sensors during the experimental measurements. Since heating measurements can be affected by external conditions, such as changes in ambient temperature, all measurements were repeated three times. Subsequently, the t-distribution was used to calculate a confidence interval of the measured temperatures with a confidence level of 95%, based on the equation:

$$x_{CI} = \bar{x} \pm t \frac{s_x}{\sqrt{n}} \tag{3}$$

with the standard deviation of the number n of measured samples and the *t*-score for the selected confidence level. The calculated confidence intervals for each measured sample and applied heating power were used for comparison with the simulation results, as shown in Fig. 6.

The temperature results presented in Fig. 5 show a small deviation between the measured and simulated values. In the simulation, the temperature difference between the two sensor positions near the tool tip is slightly lower than the measured temperatures. However, the third and fourth sensor position already show a correct course. This deviation of the simulated results from the measured temperatures, respectively from the calculated confidence intervals, at the first two sensor positions may be caused by the smaller distance to the induction coil. At this area the intensity of the electromagnetic field is higher and thus the measured or simulation-based inaccuracies may also have a larger impact than at the other two sensor positions. However, despite these deviations, the simulated temperatures still achieve sufficient accuracy for further application of this methodology.
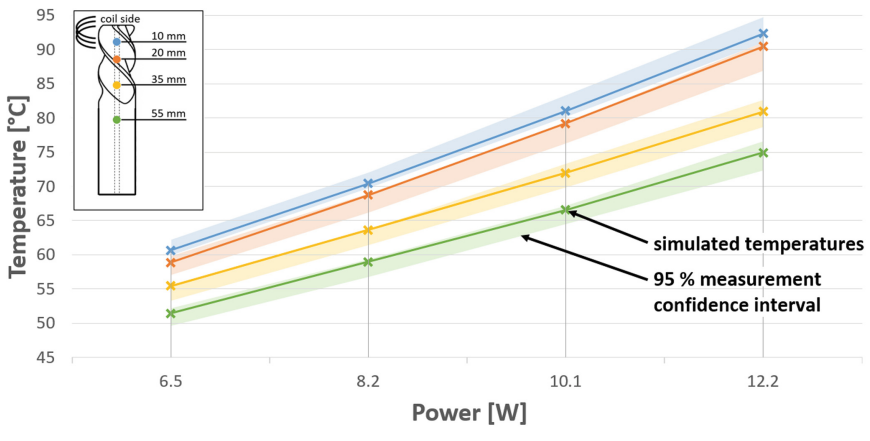
Fig. 6. Comparison of simulated temperatures with 95% confidence intervals from measured temperatures for selected power configuration

5 Summary

FSI-coupled simulations need to be verified experimentally. For this purpose, it is necessary to set a realistic and precisely defined heat input into the tool. This is not possible through a real machining process, since the simulation of the entire machining operation would be too complex. Induction heating has shown to be capable of heating a given test tool, and it is also possible to determine the induced energy through electromagnetic simulations supported by experimental measurements. By measuring the high-frequency waveform of the current flowing through the induction coil (in particular amplitude and frequency), the input values for the simulation in ANSYS Maxwell® were obtained. Simulation with the 3D models of the induction coil and the heated test tool was performed to determine the ohmic losses in the test tool, which are subsequently converted into heating power. This electromagnetic simulation was validated by measurements for a series of four different power levels. The subsequent comparison demonstrated that the measured power was higher than the simulated power. This proves the accuracy of the results, since the measured power includes P_{DC} losses that were neglected in the numerical simulation (ΔP_C, ΔP_w, ΔP_o).

The simulated ohmic losses in the test cylinder were further applied as a heat source in the thermal simulation created in ANSYS CFX. This simulation was set up to simulate the thermal heating process to prove the functionality of this methodology. A comparison of the simulated and 95% confidence intervals calculated from measured temperature values showed slight deviations, which may be caused by both the measurement inaccuracies and the simplifications of the simulation models. However, after taking into account multiple possible inaccuracies through the whole methodology, the final simulated temperatures reach approximately same values as the measured ones.

This paper proves the described methodology of the induction heating of the cutting tool and its simulation as sufficiently accurate and functional. Furthermore, a liquid cooling can be implemented into the methodology described in this paper as a last

step before the possibility of full verification of more complex FSI simulation model developed for the investigation of thermally induced displacement of the tool center point of the cutting tool under influence of a liquid coolant.

References

1. Helmig, T., Göttlich, T., Liu, H., Nguyen, N., Bergs, T., Kneer, R.: Numerical investigation on evolving chip geometry and its impact on convective heat transfer during orthogonal cutting processes. In: Proceedings of the 9th International Conference on Fluid Flow, Heat and Mass Transfer (FFHMT'22) (2022)
2. Liu, H., Peng, B., Meurer, M., Schraknepper, D., Bergs, T.: Three-dimensional multi-physical modelling of the influence of the cutting fluid on the chip formation process. Procedia CIRP **102**, 216–221 (2021)
3. Brier, S., Regel, J., Putz, M., Dix, M.: Unidirectional coupled finite element simulation of thermoelastic TCP-displacement through milling process caused heat load. MM Sci. **51**, 465–483 (2021)
4. Topinka, L., Bräunig, M., Regel, J., Putz, M., Dix, M.: Multi-phase simulation of the liquid coolant flow around rotating cutting tool. MM Sci. **5**, 5148–5153 (2021)
5. Glänzel, J.: Einzigartige Thermozelle zur Untersuchung klimatischer Effekte auf Werkzeug-maschinen, wt Werkstattstechnik online **107**, 511–512 2017
6. Regel, J.: Bewertung konstruktiver und kompensatorischer Maßnahmen zur thermo-sensitiven Auslegung von Werkzeugmaschinenstrukturen, Dissertation (2018)
7. Lammeraner, J., Stafl, M.: Eddy currents 232 (1964)
8. Hradilek, H., Laznicková, I., Kral, V.: Elektrotepelna premena 2011
9. Puyal, D., Bernal, C., Burdio, J.M., Acero, J., Millan, I.: Methods and procedures for accurate induction heating load measurement and characterization In: IEEE Xplore, pp. 805–810 (2007)
10. Park, C.Y.: Inverter efficiency analysis model based on solar power estimation using solar radiation 2020